BIOCHEMISTRY
including biophysical chemistry & molecular biology

Article

pubs.acs.org/biochemistry

Blue Light-Induced Dimerization of a Bacterial LOV–HTH DNA-Binding Protein

Brian D. Zoltowski,[†] Laura B. Motta-Mena, and Kevin H. Gardner*

Departments of Biophysics and Biochemistry, University of Texas Southwestern Medical Center, Dallas, Texas 75390-8816, United States

Supporting Information

ABSTRACT: With their utilization of light-driven allostery to control biochemical activities, photosensory proteins are of great interest as model systems and novel reagents for use by the basic science and engineering communities. One such protein, the light-activated EL222 transcription factor, from the marine bacterium *Erythrobacter litoralis* HTCC2594, is appealing for such studies, as it harnesses blue light to drive the reorientation of light–oxygen–voltage (LOV) sensory and helix–turn–helix (HTH) effector domains to allow photoactivation of gene transcription in natural and artificial systems. The protein conformational changes required for this process are not well understood, in part because of the relatively short lifetime of the EL222 photoexcited state ($\tau \sim 29$ s), which complicates its characterization via certain biophysical methods. Here we report how we have circumvented this limitation by creating an EL222 variant harboring V41I, L52I, A79Q, and V121I point mutations (AQTrip) that stabilizes the photoactivated state. Using the wild-type and AQTrip EL222 proteins, we have probed EL222 activation using a combination of solution scattering, nuclear magnetic resonance (NMR), and electromobility shift assays. Size-exclusion chromatography and light scattering indicate that AQTrip oligomerizes in the absence of DNA and selects for an EL222 dimer–DNA complex in the presence of DNA substrates. These results are confirmed in wild-type EL222 with a high-affinity DNA-binding site that stabilizes the complex. NMR analyses of the EL222–DNA complex confirm a 2:1 stoichiometry in the presence of a previously characterized DNA substrate. Combined, these novel approaches have validated a key mechanistic step, whereby blue light induces EL222 dimerization through LOV and HTH interfaces.

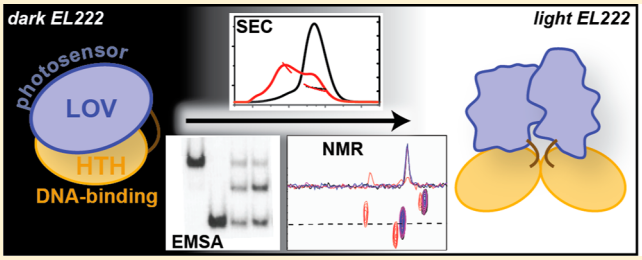

Rapid adaptation to environmental changes requires that organisms coordinate biological responses using a combination of sensory and signal transduction machinery. One sensory component, the light–oxygen–voltage (LOV) domains, allows diverse enzymatic and signaling proteins to detect changes in blue light intensity and redox state.[1,2] Despite these varied output signals, LOV proteins use a common photochemistry, as has been well studied in isolated LOV domains.[1−5] However, because only few full-length LOV sensor/signal transduction proteins have been characterized with biophysical methods, we only partly understand the mechanisms of relaying alterations within the LOV core to downstream signaling components.

Some insight into these issues is provided by recognizing that LOV domains are a subset of the larger family of Period-ARNT-Singleminded (PAS) protein/protein interaction domains, many of which are ligand-regulated themselves.[6,7] These small domains (~110 residues) adopt a common α/β-fold with a central β-scaffold flanked on one side by a series of short helices. Most ligand-regulated PAS domains typically function by binding environmentally sensitive small molecule cofactors between the helical and β-sheet secondary structures, as seen for FMN or FAD chromophores within LOV domains.[1,2,6] While these are noncovalent flavoprotein complexes in the dark, illumination leads to the formation of a covalent adduct between the C4a position of the flavin ring and the sulfur of a nearby conserved cysteine,[1,2] constituting the first step in environmental control of LOV proteins.

Subsequent signal transduction steps have been probed in an array of mechanistic studies conducted with isolated LOV domains, suggesting three general ways that structural changes triggered by adduct formation are propagated to effector domains or proteins.[1] These include light-driven (1) release of effector helices or domains, freeing them from inhibitory interactions with the LOV β-sheet,[5,8−12] (2) reorganization of flanking protein elements to allow formation of LOV–LOV dimers,[3,13] and (3) reorientation of a preexisting LOV–LOV β-scaffold-mediated dimer.[4,14,15] In all three mechanisms, adduct-induced changes to the isoalloxazine ring configuration (including protonation of N5) propagate via altered protein–flavin interactions to the LOV β-sheet.[1,8]

To fully characterize the structural and functional changes involved in LOV signaling, it is necessary to examine the light-induced biophysical and biochemical features of full-length proteins containing both sensory and effector domains. To the

Received: July 31, 2013
Revised: August 29, 2013
Published: August 30, 2013

best of our knowledge, only one natural protein meeting these criteria has provided high-resolution structural information needed for such studies: EL222, a bacterial light-regulated DNA-binding protein.[10] EL222 consists simply of an N-terminal LOV domain followed by a C-terminal NarL/LuxR-type helix−turn−helix (HTH) DNA-binding domain, suggesting it functions as a light-dependent DNA-binding protein. This was borne out by initial structural and functional characterization, showing that EL222 adopts an inactive, monomeric conformation in the dark, stabilized by inhibitory LOV−HTH contacts.[10] Upon illumination, EL222 undergoes standard LOV photochemistry and breaks these interdomain contacts, facilitating binding of EL222 to its preferred 12 bp DNA sequence, which we identified with genomic ChIP-Seq and artificial SELEX methods.[16] Within the native *Erythrobacter litoralis* HTCC2594 host, we further observed light-dependent enhanced transcription of genes located near some EL222-binding sites in the genome, suggesting that EL222 serves as an environmentally responsive transcription factor *in vivo*.

As with other LOV proteins, the mechanism of EL222 activation remains incompletely characterized. On the basis of two lines of reasoning, one facet is clear: EL222 likely oligomerizes as part of the activation process, converting from its monomeric inhibited state into a multimeric DNA-bound form. First, the activities of many proteins that contain LOV or HTH domains are regulated at the level of oligomeric complex formation and modification.[3,4,17−19] Notably, DNA binding by HTH-containing proteins occurs via such complexes,[17−19] the formation of which is often controlled by N-terminal regulatory domains. Within EL222, the dimerization surfaces typically used by both LOV (β-sheet) and HTH (4α helix) domains are occluded in the dark-state monomer, preventing their use in assembling higher-order complexes. Second, DNA-binding sites for EL222 reveal an internal repeat, consistent with binding by multiple proteins.[16] Taken together, these precedents imply that the structural changes observed upon EL222 activation[10] likely lead to oligomerization of the protein.

While this hypothesis is reasonable, its examination has been complicated by the short lifetime of the photogenerated cysteinyl−flavin adduct in EL222, hampering the application of most biophysical and biochemical methods normally used to directly observe oligomerization. Here we report how we have addressed these limitations, combining improved reagents and different techniques to obtain experimental evidence of EL222 oligomerization. We start by rationally designing variants of EL222, which extend the adduct-state lifetime, facilitating solution light scattering and gel filtration studies. These rate-altering variants reveal light-induced formation of El222 dimers that can bind DNA. Complementary experiments with wild-type EL222 and a new high-affinity DNA sequence[16] demonstrate that native EL222 also forms an EL222 dimer−DNA complex. We close by using solution NMR methods, which allow direct measurement of protein−DNA complex formation with *in situ* illumination, to examine the ability of EL222 to bind various DNA substrates. Taken together, these independent approaches directly establish that oligomerization is a key step of EL222 activation.

EXPERIMENTAL PROCEDURES

Cloning and Protein Purification. EL222 variants harboring V41I, L52I, A79Q, L120K, V121I, and S137Y mutations alone or in combination were constructed within the context of an N-terminal truncation construct (containing residues 14−222) using the QuikChange protocol (Agilent Technologies) and subcloned into the His_6-Parallel expression vector.[20] Of note, EL222 is derived from the ELI_04755 gene, but different predictions of the translation start site lead to slightly different predicted protein products. In this work and all of our prior work,[10,21] we use residue numbers assuming that translation starts at the methionine that generates a protein that begins with a MGQDR... sequence; sequences in several databases (e.g., NCBI entry YP_457840.1) have a three-residue shift by assuming an earlier methionine is used (MLDMGQDR...). Resulting variants were sequenced in their entirety (University of Texas Southwestern Sequencing Facility). WT EL222 and rate-altering variants were overexpressed in *Escherichia coli* BL21(DE3) cells grown in either Luria Broth or M9 minimal medium supplemented with 1 g/L $^{15}NH_4Cl$. Cells were grown to an OD_{600} of 0.6−0.8 prior to induction with 100 μM isopropyl thiogalactoside (IPTG) at 18 °C. Proteins were expressed for 22 h prior to being harvested.

EL222 proteins were purified by lysing cell pellets via sonication in 50 mM Tris (pH 8.0), 100 mM NaCl buffer at 4 °C before subsequent purification via Ni-Sepharose affinity chromatography. Proteins were obtained using gradient elution from 5 to 500 mM imidazole, subsequently treated with His_6-TEV protease[22] overnight at 4 °C to remove affinity tags, and subjected to another round of affinity chromatography to remove the freed His_6 tags and His_6-TEV protease. Purification was completed with a final Superdex 75 size-exclusion chromatography step, leaving samples in either 50 mM Tris (pH 8.0), 100 mM NaCl buffer (for kinetic and DNA binding studies), or 50 mM sodium phosphate (pH 6.0), 100 mM NaCl buffer (for NMR studies).

UV−Visible Absorbance Spectroscopy and Kinetics. UV−visible absorbance spectroscopy and LOV dark-state reversion kinetics were conducted on a Varian Cary 50 spectrophotometer as previously reported.[21]

Electrophoretic Mobility Shift Assay (EMSA). Experiments were conducted as described by Nash et al.,[10] using 45 bp oligomer 1 from that publication [termed AN-45 by Rivera-Cancel et al.[16] and herein (sequence listed in Table S1 of the Supporting Information)] unless otherwise noted. Briefly, ^{32}P end-labeled versions of double-stranded DNA were incubated with increasing concentrations of WT EL222 or mutant protein under either dark- or light-state conditions. Light-state WT EL222 samples were generated under a white 150 W floodlight. EL222 variants were illuminated using either an analogous illumination protocol or a series of three camera flashes while the samples were being incubated on ice. Importantly, both illumination protocols yielded identical results.

Initial assays of DNA binding were conducted with reaction mixtures containing final concentrations of 0.01 mg/mL BSA, 0.02 mg/mL poly-dI/dC, and 1.45 nM ^{32}P end-labeled AN-45 DNA (45 bp). Protein concentrations were varied between 0.1 and 20 μM, prepared in 50 mM Tris (pH 8.0), 100 mM NaCl, 2 mM $MgCl_2$, and 12% glycerol. DNA and protein mixtures were incubated on ice for 30 min in the dark or in light. Samples were then run on a 10% polyacrylamide gel in TAE buffer for 2 h at 100 V and 4 °C.

EMSA experiments to demonstrate EL222 dimerization (Figure 2c) were conducted using 1.3 nM ^{32}P end-labeled Clone-1 DNA[16] (45 bp; Figure S1a of the Supporting Information for its sequence) and an equimolar mixture of untagged EL222 and EL222 tagged with His_6-Gβ1[5] in a buffer

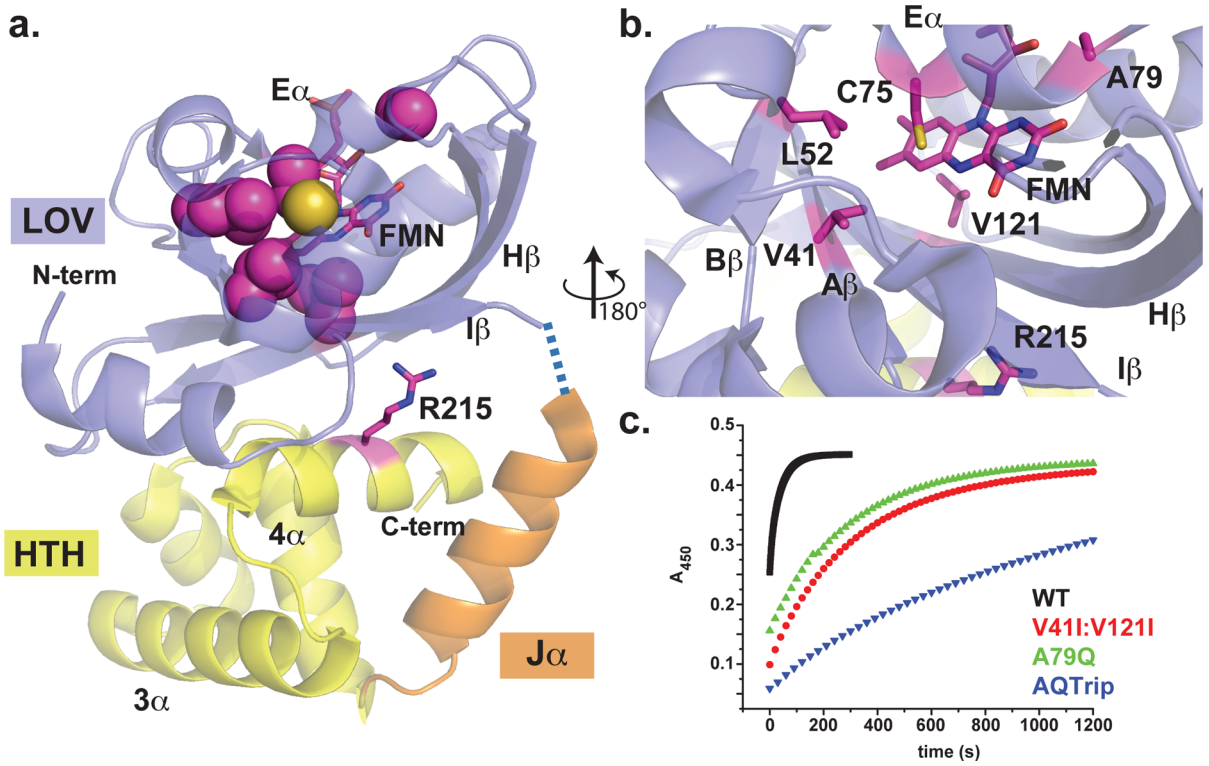

Figure 1. Active site variants of EL222 extend the lifetime of the light-state adduct. (a) EL222 consists of two folded domains: an N-terminal LOV domain (blue) coupled by a connecting Jα helix (orange) to a C-terminal HTH DNA-binding domain (yellow). The dark-state crystal structure[10] shows that the LOV β-sheet directly contacts the 4α dimerization helix of the HTH domain; photochemically induced adduct formation involving the FMN (magenta sticks) within the LOV domain causes conformational changes that perturb the LOV–HTH interaction, as demonstrated by large light-induced chemical shift changes in R215 (magenta sticks) following photoexcitation.[10] Variants identified to date that alter the lifetime of the photochemically generated adduct are confined to residues whose side chains directly protrude into the FMN-binding cavity (magenta spheres for carbon atoms of these side chains; the yellow sphere indicates the location of the Sγ atom of C75). (b) An expansion of the structure in panel a shows the residues localized to the active site that when mutated affect the lifetime of the light-state adduct. V41I and L52I alter interactions with both the adduct-forming C75 and the active site FMN, while V121I is positioned at the *re*-face of the flavin and regulates flavin reduction potentials in VVD.[27] A79 is located in a surface Eα–Fα loop and directly contacts the flavin chromophore; however, the A79Q variant alters H-bonds at the flavin N1 position and directly stabilizes the light-state adduct.[21] (c) Dark-state reversion rates were determined by fitting the absorbance at 450 nm after illumination. EL222 variants tune the lifetime of the adduct state relative to WT (black; $\tau \sim 29$ s at 25 °C),[21] with V41I/V121I (red) and A79Q (green) both increasing the lifetime of the adduct state 10-fold ($\tau \sim 300$ s). Combining these mutations with a further L52I variation increases the lifetime to a maximum of ~2000 s in a V41I/L52I/A79Q/V121I (AQTrip, blue) variant.

containing (final concentrations) 0.01 mg/mL BSA, 0.025 mg/mL poly-dI/dC, 10 mM Tris (pH 8.0), 80 mM NaCl, 3 mM $MgCl_2$, and 10% glycerol. Reaction mixtures were incubated under light conditions for 25 min on ice and then run on a native 5% acrylamide gel in TAE at 150 V for 2 h at 4 °C.

NMR Titration Experiments. NMR-based titration experiments were conducted by collecting solution $^{15}N-^{1}H$ HSQC spectra[23] on samples of 80 μM ^{15}N-labeled EL222 in the presence of increasing concentrations of DNA oligos (described below) and 25 mM sodium phosphate (pH 6.0), 50 mM NaCl buffer. Data were collected in the presence and absence of DNA oligos ranging from 15 to 45 bp at concentrations ranging from 5 to 100 μM. Oligos were based on 5′ and 3′ truncations of AN-45, generating AN-15–AN-35 (Figure S1a of the Supporting Information). All spectra were collected at 25 °C on Varian 600 and 800 MHz spectrometers equipped with cryogenically cooled ^{15}N, ^{13}C, ^{1}H triple-resonance probes. Light-state samples were collected as described previously.[10] All data were processed using NMRPipe[24] and analyzed using NMRViewJ.[25]

Fractional EL222 occupancies were quantified by ratios of peak intensities for 35 light-state peaks of EL222, previously assigned to specific residues in the protein.[10] For the purpose of quantification, peak intensities in the absence of DNA (control) were assigned a concentration of 80 μM. The concentration of free protein at each DNA concentration was thus

$$[\text{free EL222}] = 80\ \mu\text{M} \times [\text{peak}]_{+\text{DNA}} / [\text{peak}]_{\text{control}} \quad (1)$$

The resultant fraction bound was then

$$\text{fraction protein bound} = 1 - [\text{free EL222}]/80\ \mu\text{M} \quad (2)$$

The calculated fractional protein bound was averaged over all 35 peaks to reduce random error.

To evaluate binding affinities and stoichiometries in a length-independent manner, DNA concentrations were normalized to the relative concentration of 20 bp equivalents. The concentrations of 20 bp equivalents were calculated by the following equation:

$$\text{normalized } [\text{DNA}] = ([\text{DNA}] \times \text{number of base pairs})/20 \quad (3)$$

DNA titrations were then plotted with normalized [DNA] and actual [DNA] and fit with a one-site-specific, cooperative

dx.doi.org/10.1021/bi401040m | *Biochemistry* 2013, 52, 6653–6661

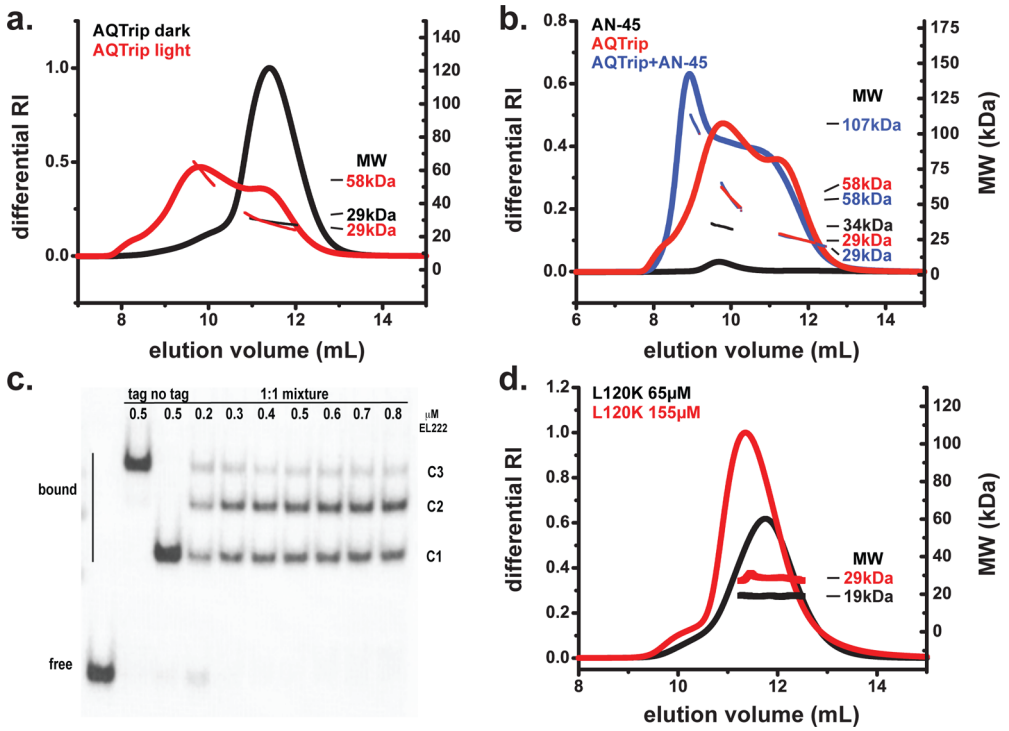

Figure 2. Dimerization of EL222 variants both free in solution and bound to DNA. (a) SEC−MALLS measurements of dark- and light-state AQTrip indicate the light-driven formation of a dimeric species. Under dark-state conditions, AQTrip is largely monomeric (black) at the concentration used (140 μM). In contrast, at equivalent concentrations, AQTrip is a mixture of the monomer and dimer in the light state (red). (b) Mixtures of 120 μM light-treated AQTrip and 60 μM AN-45 DNA result in the formation of a species (blue) that elutes more rapidly than light-state AQTrip alone (red) and DNA alone (black). The molecular mass of the light-state DNA-bound EL222 complex is consistent with a 2:1 EL222:DNA ratio. (c) EMSA analysis of interactions of EL222 with Clone-1 DNA[16] (see Figure S1a of the Supporting Information for its sequence), conducted in the presence of His_6-Gβ1-tagged and untagged WT EL222, confirms a 2:1 stoichiometry for EL222−DNA interactions. The presence of a mixed species (C2) compared to tagged (C3) and untagged (C1) protein−DNA complexes indicates that EL222 dimers interact with this 45 bp oligo. The lack of additional bands suggests monomeric or larger oligomeric states do not bind appreciably at the concentrations tested. (d) L120K is monomeric (molecular mass of 19 kDa) under dark-state conditions at 65 μM (black). Increasing the concentration to 155 μM (red) results in a small shift in both elution time and molecular mass, up to an ~29 kDa species, consistent with a rapidly exchanging low-affinity dimer.[27,30] For panels a, b, and d, each graph includes both UV absorbance measurements (top lines) and MALLS traces (bottom lines); molecular mass measurements are provided from the midpoint of the MALLS traces shown.

binding model as provided in GraphPad Prism (GraphPad Software).

The reversibility of DNA binding was quantified by comparing the initial peak intensities of the dark-state locations of these 35 assigned residues before illumination and again after a dark−light−dark cycle. These data were compared to those of an analogous experiment conducted in the absence of DNA to separate the effects of the illumination protocol from DNA binding. Data for A79Q were collected at a protein concentration of 140 μM with 70 μM AN-35.

Size-Exclusion Chromatography−Multiangle Laser Light Scattering (SEC−MALLS). Determination of the absolute molecular mass of light-state and DNA-bound complexes were determined using SEC−MALLS experiments. All SEC−MALLS experiments were conducted on a mini-DAWN Treos static light scattering instrument (Wyatt) equipped with an in-line refractive index detector. All experiments were conducted on 400 μL samples with protein concentrations varying from 40 to 350 μM and DNA concentrations of up to 60 μM. Samples were injected onto a Superdex 75 (10/300) analytical gel filtration column to separate oligomeric species and protein aggregates. Light-state data were collected by first illuminating samples with three successive camera flashes immediately prior to injection. Molecular mass determinations were subsequently determined via in-line MALLS detection and calculated using Wyatt Astra software.

RESULTS

Utility of Rate-Altering EL222 Mutants. Our prior studies of EL222 revealed that it has a relatively short-lived photochemically generated adduct (τ = 29 s at 25 °C),[21] particularly when its lifetime is compared to the times required for commonly used methods for evaluating DNA binding and stoichiometry (e.g., EMSA and size-exclusion chromatography). The short lifetime of the EL222 active state thus introduces several practical complications into measurements of EL222−DNA interactions, from the need to utilize constant illumination to challenges with the detection of relatively short-lived species with different biophysical methods. To address these experimental issues, we used EL222 variants that contain point mutations, which stabilize the light-state adduct, and used these to discern the stepwise process of EL222 photoactivation and DNA recognition.

Comparable rate-altering variants have been characterized in several LOV proteins;[21,26,27] in particular, variants of the *Neurospora crassa* Vivid (VVD) protein can modulate the active-state lifetime over 4 orders of magnitude without

dx.doi.org/10.1021/bi401040m | *Biochemistry* 2013, 52, 6653−6661

affecting the *in vitro* function of the protein.[27] Building from this foundation, we compared the EL222 and VVD LOV domain sequences and identified three positions at which VVD mutations alter the lifetime of the C4a adduct [EL222 residues V41, L52, and V121 (Figure 1 and Figure S2 of the Supporting Information)]. Given that these mutations were found to modulate adduct-state stability in VVD, AsLOV2, and YtvA across several orders of magnitude,[26−29] we resolved to target the analogous residues in EL222 for mutagenesis. Interestingly, analysis of the sequence immediately surrounding the critical LOV cysteine residue revealed an additional substitution at the Gln residue usually found here (canonical GRNCRFL***Q*** vs GRNCRFL***A*** in EL222); mutations of this site (A79Q)[21] or nearby hydrophobic residues (V41I/V121I) each slow the adduct cleavage rate by an order of magnitude compared to the rate of the wild-type protein (Figure 1c). Combining these mutations with a change at another nearby hydrophobic site (V41I/L52I/A79Q/V124I, termed AQTrip) revealed some additivity among these effects, culminating in a stabilized adduct that decayed with a time constant of ∼2000 s (Figure 1c). While this ∼70-fold attenuation of adduct cleavage observed in AQTrip is not as large as that observed in some other LOV systems,[27] it is more than sufficient for biophysical studies of oligomerization and DNA recognition in EL222. Because the mechanisms of adduct-rate attenuation of these types of mutations in VVD, AsLOV2, and YtvA have been analyzed in detail elsewhere,[26−29] and also in EL222,[21] they will not be discussed here.

Characterization of the Oligomeric State of a Slow-Cycling EL222 Variant. As noted above, LOV and HTH proteins are often regulated by controlling the protein oligomeric state. To test if such a regulatory model holds for EL222, we used size-exclusion chromatography coupled to multiangle laser light scattering (SEC−MALLS) to probe the oligomeric state of light-state EL222 in the presence and absence of a double-stranded DNA substrate. As expected, SEC−MALLS data show that dark-state AQTrip elutes as a monomer (Figure 2a), with a MALLS-determined molecular mass of 29 kDa, which is close to the theoretical mass of 24 kDa. Following photoexcitation, AQTrip elutes as a mixture of three species: a monomeric 29 kDa form consistent with dark-state AQTrip, a 58 kDa dimeric complex, and a rapidly eluting high-molecular mass species (Figure 2a). Notably, the apparent molecular mass of the oligomer is concentration-dependent, indicative of a rapid monomer−dimer equilibrium (Figure S3 of the Supporting Information) as observed for several other PAS-containing proteins.[3,30] Increasing the protein concentration to 300 μM results in the formation of a light-state tetramer (Figure S3 of the Supporting Information). Thus, at high concentrations, stabilized forms of EL222 are capable of light-induced oligomerization in the absence of DNA.

To determine how the light-induced oligomerization is involved in DNA recognition, we conducted analogous SEC−MALLS experiments on light-state AQTrip in the presence of DNA (Figure 2b). Taking advantage of the previously characterized AN-45 substrate for EL222,[10,16] we used this double-stranded oligo in our SEC−MALLS experiments. As in experiments conducted in the absence of DNA, we observed three species in the AQTrip−DNA samples. The predominant species eluted more rapidly than either free DNA or light-state AQTrip oligomers with a molecular mass of ∼107 kDa, consistent with a 2:1 protein:DNA ratio [predicted molecular mass of 92 kDa (Figure 2b)]. The two additional species eluted with masses of 58 and 29 kDa, consistent with free dimeric and monomeric EL222, respectively. Unfortunately, while sample constraints complicated the reproduction of these results at protein and DNA concentrations sufficient to observe putative tetrameric species (350 μM protein and >100 μM DNA), it is readily apparent from these data that a DNA-bound protein tetramer is not the preferred configuration.

Characterization of Wild-Type and Constitutively Active EL222 Oligomerization. While comparable SEC−MALLS experiments with wild-type (WT) EL222 protein were complicated by the short lifetime of the light state, we were able to use EMSA experiments with samples containing mixtures of His_6-Gβ1-tagged and untagged WT EL222 to demonstrate the presence of mixed dimeric states on DNA (Figure 2c). For these experiments, we used a different DNA substrate called Clone-1, a higher-affinity 45 bp duplex (EC_{50} ∼ 0.3 μM), which we identified with SELEX-based selection among a pool of artificial DNA sequences.[16] Similar to our SEC−MALLS experiments with AQTrip, EMSA analysis of WT protein with the Clone-1 DNA revealed analogous EL222 dimer−DNA interactions. Importantly, three DNA-bound complexes were observed: a rapidly migrating species consistent with an untagged protein dimer (labeled C1), a slower-migrating species similar to a His_6-Gβ1-tagged protein dimer (labeled C3), and an intermediate species representative of a His_6-Gβ1-tagged−untagged protein complex (labeled C2) (Figure 2c). Given the lack of additional species, we conclude that EL222 preferentially interacts with DNA as a dimer and not as monomer or tetramer. Taken together, our SEC−MALLS and EMSA data demonstrate the light-induced formation of an EL222 dimer that is capable of binding to DNA.

Although we cannot identify the protein−protein interface(s) used to assemble the EL222 dimer complex using SEC−MALLS alone, precedence from other LOV and HTH structures does suggest candidates for these interfaces, allowing us to predict mutations in EL222 that disrupt the observed dark-state LOV−HTH packing and produce constitutively active, DNA-binding variants that can provide some insight into structures involved in light-induced dimerization.[10] Two such variants, L120K and S137Y, both alter residues on the LOV β-sheet adjacent to the HTH 4α helix[10] (Figure S4a of the Supporting Information). The L120K variant, which we have shown to bind AN-45 in the dark with an affinity comparable to that of light-state WT protein,[10] appears to be in a rapid exchange between monomeric and dimeric states as shown by the concentration dependence of its SEC elution profile and apparent molecular mass (Figure 2D). EMSA analysis indicates that S137Y also binds AN-45 in the dark with an affinity comparable to that of illuminated WT protein (Figure S4b of the Supporting Information) and appears to be in a monomer−dimer equilibrium based on SEC−MALLS results (Figure S4c of the Supporting Information). These data suggest that both mutations activate EL222 by releasing the inhibitory LOV−HTH interactions observed in the dark-state crystal structure, but their introduction of charge and/or steric constraints does not preclude the (albeit transient) formation of EL222 dimers. Such behavior is consistent with dimerization being driven by HTH−HTH interactions with potential side contributions from LOV−LOV dimerization.

DNA Recognition by WT EL222 and Rate-Altering Variants. While SEC−MALLS and EMSA analysis of WT and rate-altering variants indicate that dimer formation is required for DNA binding, these experiments did not address the

potential impact of the rate-altering variants on the affinity of these interactions. We initially evaluated DNA binding via EMSA analyses in a manner analogous to that of the experiments conducted with WT EL222 and A79Q variant.[10,21] Light-state EMSAs revealed that all of the variants inspected (A79Q, V41I/A79Q, and AQTrip) bound AN-45 with an affinity equivalent to (V41I/A79Q) or higher than (A79Q and AQTrip) that established for WT EL222 (EC_{50} ~ 8 μM) (Figure S5 of the Supporting Information). In addition, two variants (V41I/A79Q and A79Q) formed supershifted bands that had been seen with WT EL222 only at high protein concentrations (>20 μM) and the constitutively active L120K variant.[10] Thus, mutations within the flavin-binding pocket have the potential for generating allosteric changes in the surrounding LOV domain that may impart increased affinity for DNA.

To complement these EMSA measurements with a solution method in which illumination could be more readily controlled in real time, we developed an alternative NMR-based DNA binding assay. Initial $^{15}N-^{1}H$ HSQC spectra of uniformly ^{15}N-labeled WT EL222 in the dark showed minimal, concentration-independent effects on peak shifts or intensity without or with AN-45 duplex DNA, confirming the lack of DNA binding (at concentrations up to 80 μM) for dark-state WT EL222 (data not shown). In contrast, titration of AN-45 DNA into illuminated EL222 samples yielded a substantial DNA-dependent loss of peak intensity (Figure 3a). Such changes are consistent with binding of EL222 to AN-45 under these conditions, with line broadening caused by the slowed rotational diffusion of the complex, intermediate chemical exchange broadening, or both. Within these samples, more than 90% of the signal intensity was restored after returning to dark-state conditions postillumination, confirming the reversibility of DNA binding by EL222 (Figure 3b,c). Quantifying peak intensities following dark–light–dark cycles, in the presence and absence of either AN-45 or a shorter 35 bp AN-35 fragment (Figure S1 of the Supporting Information), we established that the minimal loss of signal intensity was not a consequence of DNA (Figure 3b, inset one-dimensional traces) and was not affected by the presence of the A79Q mutation (Figure 3c).

Further quantitation of the intensities of 35 assigned light-state WT EL222 peaks[10] as a function of AN-45 concentration provided additional confirmation of the 2:1 EL222:DNA stoichiometry observed in EMSA and SEC–MALLS analyses. Specifically, we observed a progressive loss of peak intensity with the titration of AN-45 into 80 μM WT EL222, with a complete loss of peak intensity occurring at approximately 40 μM AN-45 (Figure 4). Saturation at this concentration is consistent with two EL222-binding sites per DNA molecule (Figure 4a), as expected from our experimental data and the presence of two half-sites within the consensus EL222-binding site found by ChIP-Seq and SELEX[16] (Figure S1 of the Supporting Information). In addition, fitting the titration data to an equation for potentially cooperative, specific binding to a single site yields an apparent K_D of ~11 μM for AN-45, similar to the EC_{50} established by EMSA (~8 μM) despite significant differences in the experimental conditions and approaches used to obtain these values.

With these initial validations of the NMR-based approach for examining EL222–DNA complexes, we used this method to examine the effect of truncating the AN-45 oligo on EL222 binding affinity. Titrations of 15–45 bp fragments of AN-45

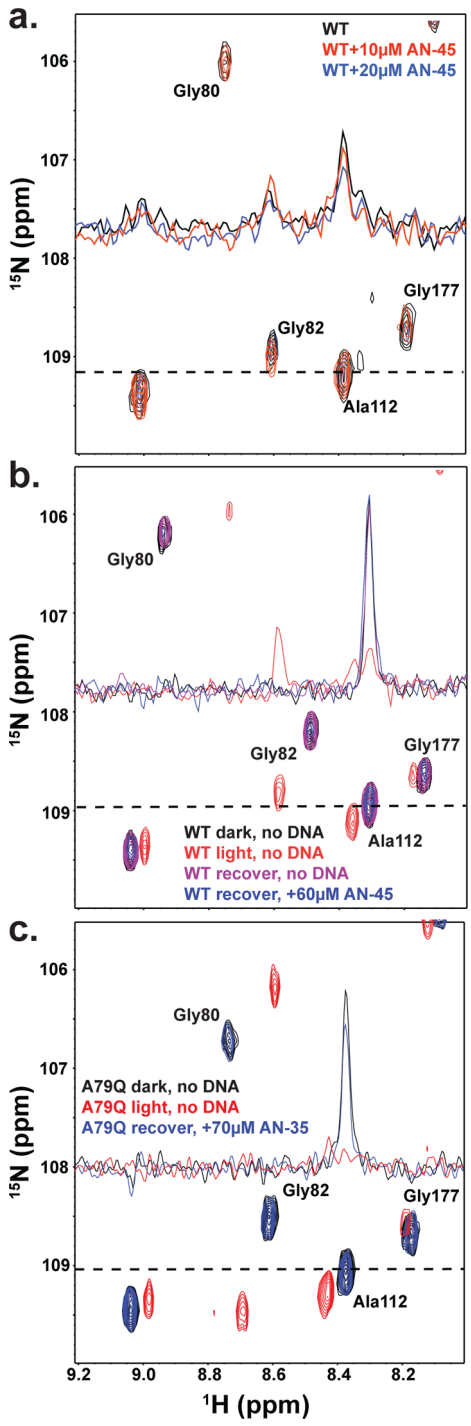

Figure 3. NMR-based DNA binding studies show reversible binding of EL222 to DNA. (a) EL222 binding to DNA can be monitored by titrating increasing amounts of AN-45 DNA into ^{15}N-labeled EL222 and analyzing peak intensities in $^{15}N-^{1}H$ HSQC light-state spectra. Dashed lines represent the locations of the cross section used for the one-dimensional trace shown in the inset. Addition of 10 μM AN-45 (red) and 20 μM AN-45 (blue) to 80 μM WT EL222 decreases the intensity of all peaks relative to the intensity of those of light-state WT EL222 protein alone (black) in a concentration-dependent manner. Loss of peak intensity is consistent with binding of EL222 to AN-45 DNA. (b) Initial WT EL222 dark-state peak intensities (black) are comparable to peak intensities following a dark–light–dark cycle in the presence (blue) and absence of DNA (magenta). A light-state spectrum of EL222 (red) in the absence of DNA is shown for comparison. An up to 30% loss of peak intensity is observed in some

dx.doi.org/10.1021/bi401040m | *Biochemistry* 2013, 52, 6653–6661

Figure 3. continued

experiments even in the absence of DNA; however, for all experiments, the loss of peak intensity is similar between DNA and DNA-free samples. Concentration-independent loss of peak intensity between dark-state spectra with and without DNA indicates that only minimal interaction occurs between EL222 and DNA in the dark. (c) DNA binding is also reversible with A79Q (140 μM) when AN-35 DNA (70 μM) is present (blue), which is evident from the absence of peaks observed with light-state A79Q alone (red). Peaks for dark-state A79Q (black) were similar to peaks observed with recovered A79Q in the presence of AN-35 DNA.

DNA into EL222 (80 μM) revealed substantial differences in saturation and apparent binding affinities among these fragments (Figure 4a and Figure S1a of the Supporting Information). The effects of truncation of the 5′ and 3′ ends of AN-45 on the apparent affinity and saturation are most evident with the AN-15 substrate, which showed minimal, nonsaturated DNA binding above the dark-state threshold (Figure 4a). Intermediate truncations affected both the affinity and minimal saturating concentration of EL222 in a rational manner. The effects on affinity are best seen in plots of protein bound as a function of DNA concentration normalized to the total concentration of available base pairs in all oligos (Figure 4b), allowing discrimination among sequence-specific or nonspecific binding. When normalized, AN-45 shows a modest increase in binding affinity compared to those of AN-20, -30, and -35, whose titration profiles were superimposable. AN-15 showed no effective binding. Analysis of the AN-45 sequence reveals some homology to the consensus EL222-binding site[16] at the 3′ terminus (Figure S1 of the Supporting Information), whereas this site is either flanked by a sole base pair (AN-35) or abolished altogether (AN-20 and -25) in the truncated variants. In AN-15, the lack of effective binding likely reflects the fact that the DNA is too short to allow recognition by the EL222 dimer. Plots of total protein bound as a function of DNA (Figure 4c) complement these analyses and provide additional insight into the recognition of AN-45 by EL222. Analysis of the slopes of protein concentration versus DNA concentration indicates that only AN-45 is saturated with two EL222 molecules per DNA, consistent with our prior SEC−MALLS and EMSA data. AN-35 is intermediate between a single copy and a dimeric unit; shorter DNAs bound only a single EL222 molecule on average. Taken together, we interpret these data to reflect the effects of truncating the 3′ terminal sequence on decreasing both the affinity and the preferred stoichiometry of the EL222−DNA interaction.

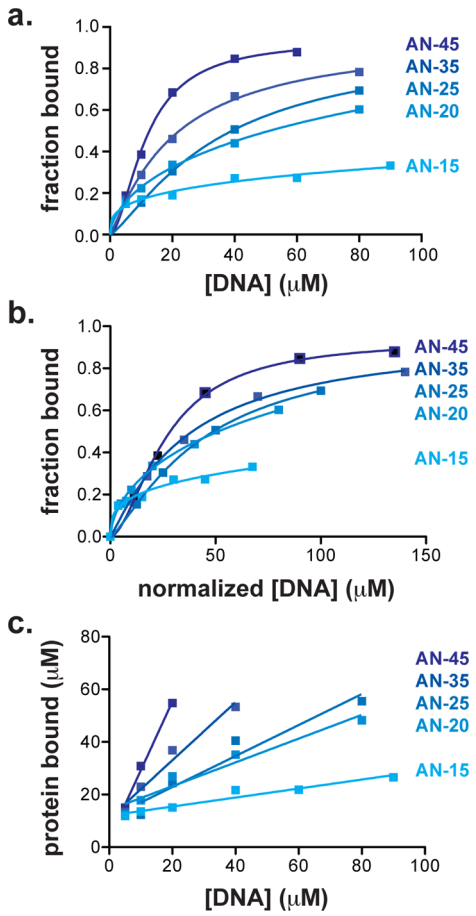

Figure 4. Quantification of the affinity and stoichiometry of DNA binding in EL222 from NMR-based studies. (a) Peak intensities obtained from NMR-based titration experiments were plotted as a function of DNA concentration. Five substrates all derived from the original 45 bp AN-45 DNA were tested for binding to WT EL222. Truncation of the ends by 5 bp each to create a 35 bp oligo [AN-35 (Figure S1a of the Supporting Information)] has a minor negative effect on DNA binding. Further truncations to a 25-mer (AN-25) or a 20-mer (AN-20) have larger effects, while both retain some binding to EL222. Binding is essentially lost in a 15-mer (AN-15). All curves were fit with a single-site-specific binding curve, including a Hill coefficient for cooperativity. (b) Normalization of the DNA concentration in panel a to the number of 20 bp equivalents suggests that AN-45, -35, -25, and -20 have similar binding efficiencies. (c) Comparisons of EL222 protein bound as a function of DNA concentration indicate that smaller oligos do not bind with the same stoichiometry. On average, two protein molecules bind to the complete 45 bp AN-45 oligo; however, only one molecule binds efficiently to AN-25 and AN-20. AN-35 exhibits an efficiency intermediate between the efficiencies of these cases, consistent with its inclusion of a DNA sequence resembling a consensus EL222-binding site at the 3′ terminus of AN-45.

DISCUSSION

As stated at the outset, our understanding of the mechanistic basis of environmental sensing and signaling within protein receptors requires knowledge of stimulus-triggered structural, dynamic, and functional changes. Within the LOV class of photoreceptors, such studies have been slowed in part by the lack of full-length proteins, containing both LOV and effectors, that are suitable for high-resolution biophysical and biochemical characterization. While two engineered "optogenetic" tools have recently provided some understanding of how LOV domains might be adapted to control small GTPases and histidine kinases,[15,31] there is a clear need to complement this work by examining natural proteins. Accordingly, we have focused on the EL222 LOV−HTH protein,[10] which can provide insight into natural regulatory processes as well as broaden our understanding of how LOV domains regulate different biochemical activities.

Coupling precedence from other LOV and HTH proteins with initial biophysical characterization,[10] we found it was relatively straightforward to develop a regulatory model for EL222: Dark-state interactions between the LOV β-sheet and HTH 4α helix inhibit the DNA binding capability of this protein, in part by holding it in an inactive monomeric conformation. A combination of biophysical and biochemical

dx.doi.org/10.1021/bi401040m | *Biochemistry* 2013, 52, 6653−6661

data establish that EL222 activation proceeds through light-induced disruption of the LOV β-sheet−HTH 4α helix interactions, with the ability of several β-sheet mutations to constitutively activate EL222 DNA binding further supporting this concept.[10,21] However, a critical aspect of the model, dimerization of activated EL222, remained unproven to date, in part because of complications with the rapid decay kinetics of the photoexcited state hampering direct physical observation of this state.

Here, we address this shortcoming by using variants of EL222 with long-lived active states in EMSA, SEC−MALLS, and NMR experiments. Data derived from these experiments revealed that EL222 binds to DNA as a dimer and uses a consensus EL222-binding site similar to one we have previously reported.[16] We emphasize that prior technical challenges were addressed through three advances: (1) development of EL222 variants with longer-lived photoexcited states,[21] allowing SEC−MALLS (Figure 2), (2) identification of an artificially selected DNA oligomer with an affinity ∼20-fold higher than that of our original candidate-based AN-45,[16] allowing EMSA-based observation of mixed dimers bound to DNA [Figure 2c; comparable studies of AN-45 show a smear of mixed dimers rather than distinct bands, consistent with rapid exchange (data not shown)], and (3) utilization of solution NMR methods to examine protein−DNA complexes in equilibrium with the ability to easily photoactivate samples and without requiring separation of free protein from protein−DNA complexes.

Taken together, these results provide a model for the DNA activation process in EL222, where activation of EL222 is similar to that of other characterized HTH proteins in the NarL/LuxR class of tetrahelical HTH DNA-binding proteins. While the regulatory processes of NarL and LuxR themselves are more complex because of the involvement of a separate sensor histidine kinase, other cases clearly document how an activatable, inhibitory domain (e.g., LOV, phosphoacceptor) docks to the HTH domain in a configuration not suitable for DNA recognition.[10,32] Upon phosphorylation or light activation, the inhibitory surface is released, allowing for dimerization and DNA binding.[32] Interestingly, different proteins in the HTH class utilize different elements for dimerization: some primarily use the HTH 4α helix (e.g., NarL[32]), while others utilize N-terminal domains as mediators of dimerization (e.g., LuxR and TraR[33−35]).

Within EL222, both types of potential dimerizing domains are present, leaving open the possibility that either or both are involved in dimer formation. The LOV−PAS β-scaffold is a known mediator of protein−protein interactions and is the primary dimerization interface in several hetero- and homodimeric LOV proteins.[3,4] Our constitutively active point mutants of the EL222 LOV domain (L120K and S137Y) both exhibit some dark-state dimerization, albeit with apparently different exchange kinetics. This implies some role for the LOV domain in assembling these dimers, but with some degree of flexibility to accommodate these point mutations. Similar effects have been observed in β-sheet point mutants in other PAS dimeric systems (e.g., *Bacillus subtilis* KinA PAS-A[30]). In addition to these effects on free proteins, we suggest that the DNA scaffold will likely facilitate oligomerization, as well.

Together, our data indicate that photoactivation of EL222 follows a three-step process. First, photochemical excitation results in C4a-flavin adduct formation and subsequent alterations in local structure. Propagation of conformational changes within the LOV β-sheet then alters LOV−HTH interactions in the vicinity of S137 and L120. Finally, the elongated monomeric form can then assemble with some combination of LOV−LOV- and HTH−HTH-mediated dimers that directly recognize DNA. A return to dark-state conditions results in rapid DNA release with kinetics determined by the LOV photocycle. A detailed understanding of the molecular mechanisms of the light-activated DNA-binding protein described in this study should help to provide further insight into signal transduction and also facilitate the adaptation of EL222 into a "natural", minimally engineered photoswitchable system for use in various applications.

■ ASSOCIATED CONTENT

Ⓢ Supporting Information

All DNA sequences used in this study (Figure S1), a sequence alignment of EL222 and VVD LOV domains (Figure S2), SEC−MALLS profiles of light-state AQTrip (Figure S3), SEC−MALLS and EMSA analysis of a constitutively active S137Y variant (Figure S4), and EMSA analyses of rate-altered EL222 variants (Figure S5). This material is available free of charge via the Internet at http://pubs.acs.org.

■ AUTHOR INFORMATION

Corresponding Author

*E-mail: kevin.gardner@utsouthwestern.edu. Phone: (214) 645-6365.

Present Address

[†]B.D.Z.: Department of Chemistry, Southern Methodist University, Dallas, TX 75275.

Funding

We gratefully acknowledge funding from the National Institutes of Health (R01 GM081875 to K.H.G. and F32 GM090671 supporting B.D.Z.) and the Robert A. Welch Foundation (I-1424 to K.H.G.) in support of this research.

Notes

The authors declare no competing financial interest.

■ ACKNOWLEDGMENTS

We thank Giomar Rivera-Cancel and Abigail Nash for helpful discussions about EL222−DNA interactions and all members of the Gardner laboratory for useful comments.

■ ABBREVIATIONS

LOV, light−oxygen−voltage; SEC−MALLS, size-exclusion chromatography−multiangle laser light scattering; NMR, nuclear magnetic resonance; EMSA, electrophoretic mobility shift assay; HTH, helix−turn−helix; FMN, flavin mononucleotide; PAS, Period-ARNT-Singleminded; oligo, oligonucleotide; AQTrip, EL222 variant with V41I, L52I, A79Q, and V124I point mutations.

■ REFERENCES

(1) Zoltowski, B. D., and Gardner, K. H. (2011) Tripping the Light Fantastic: Blue-Light Photoreceptors as Examples of Environmentally Modulated Protein-Protein Interactions. *Biochemistry 50*, 4−16.

(2) Crosson, S., Rajagopal, S., and Moffat, K. (2003) The LOV domain family: Photoresponsive signaling modules coupled to diverse output domains. *Biochemistry 42*, 2−10.

(3) Zoltowski, B. D., and Crane, B. R. (2008) Light activation of the LOV protein vivid generates a rapidly exchanging dimer. *Biochemistry 47*, 7012−7019.

(4) Moglich, A., and Moffat, K. (2007) Structural basis for light-dependent signaling in the dimeric LOV domain of the photosensor YtvA. *J. Mol. Biol. 373*, 112−126.
(5) Harper, S. M., Neil, L. C., and Gardner, K. H. (2003) Structural basis of a phototropin light switch. *Science 301*, 1541−1544.
(6) Taylor, B. L., and Zhulin, I. B. (1999) PAS domains: Internal sensors of oxygen, redox potential, and light. *Microbiol. Mol. Biol. Rev. 63*, 479−506.
(7) Henry, J. T., and Crosson, S. (2011) Ligand Binding PAS Domains in a Genomic, Cellular, and Structural Context. *Annu. Rev. Microbiol. 65*, 261−286.
(8) Halavaty, A. S., and Moffat, K. (2007) N- and C-terminal flanking regions modulate light-induced signal transduction in the LOV2 domain of the blue light sensor phototropin 1 from *Avena sativa*. *Biochemistry 46*, 14001−14009.
(9) Alexandre, M. T., Domratcheva, T., Bonetti, C., van Wilderen, L. J., van Grondelle, R., Groot, M. L., Hellingwerf, K. J., and Kennis, J. T. (2009) Primary reactions of the LOV2 domain of phototropin studied with ultrafast mid-infrared spectroscopy and quantum chemistry. *Biophys. J. 97*, 227−237.
(10) Nash, A. I., McNulty, R., Shillito, M. E., Swartz, T. E., Bogomolni, R. A., Luecke, H., and Gardner, K. H. (2011) Structural basis of photosensitivity in a bacterial light-oxygen-voltage/helix-turn-helix (LOV-HTH) DNA-binding protein. *Proc. Natl. Acad. Sci. U.S.A. 108*, 9449−9454.
(11) Lungu, O. I., Hallett, R. A., Choi, E. J., Aiken, M. J., Hahn, K. M., and Kuhlman, B. (2012) Designing photoswitchable peptides using the AsLOV2 domain. *Chem. Biol. 19*, 507−517.
(12) Freddolino, P. L., Gardner, K. H., and Schulten, K. (2013) Signaling mechanisms of LOV domains: New insights from molecular dynamics studies. *Photochem. Photobiol. Sci. 12*, 1158−1170.
(13) Zoltowski, B. D., Schwerdtfeger, C., Widom, J., Loros, J. J., Bilwes, A. M., Dunlap, J. C., and Crane, B. R. (2007) Conformational switching in the fungal light sensor Vivid. *Science 316*, 1054−1057.
(14) Moglich, A., Ayers, R. A., and Moffat, K. (2009) Design and signaling mechanism of light-regulated histidine kinases. *J. Mol. Biol. 385*, 1433−1444.
(15) Diensthuber, R. P., Bommer, M., Gleichmann, T., and Moglich, A. (2013) Full-length structure of a sensor histidine kinase pinpoints coaxial coiled coils as signal transducers and modulators. *Structure 21*, 1127−1136.
(16) Rivera-Cancel, G., Motta-Mena, L. B., and Gardner, K. H. (2012) Identification of natural and artificial DNA substrates for light-activated LOV-HTH transcription factor EL222. *Biochemistry 51*, 10024−10034.
(17) Maris, A. E., Sawaya, M. R., Kaczor-Grzeskowiak, M., Jarvis, M. R., Bearson, S. M., Kopka, M. L., Schroder, I., Gunsalus, R. P., and Dickerson, R. E. (2002) Dimerization allows DNA target site recognition by the NarL response regulator. *Nat. Struct. Biol. 9*, 771−778.
(18) Jeon, Y., Lee, Y. S., Han, J. S., Kim, J. B., and Hwang, D. S. (2001) Multimerization of phosphorylated and non-phosphorylated ArcA is necessary for the response regulator function of the Arc two-component signal transduction system. *J. Biol. Chem. 276*, 40873−40879.
(19) Gautam, U. S., Chauhan, S., and Tyagi, J. S. (2011) Determinants outside the DevR C-terminal domain are essential for cooperativity and robust activation of dormancy genes in *Mycobacterium tuberculosis*. *PLoS One 6*, e16500.
(20) Sheffield, P., Garrard, S., and Derewenda, Z. (1999) Overcoming expression and purification problems of RhoGDI using a family of "parallel" expression vectors. *Protein Expression Purif. 15*, 34−39.
(21) Zoltowski, B. D., Nash, A. I., and Gardner, K. H. (2011) Variations in protein-flavin hydrogen bonding in a light, oxygen, voltage domain produce non-Arrhenius kinetics of adduct decay. *Biochemistry 50*, 8771−8779.
(22) Blommel, P. G., and Fox, B. G. (2007) A combined approach to improving large-scale production of tobacco etch virus protease. *Protein Expression Purif. 55*, 53−68.
(23) Kay, L. E., Keifer, P., and Saarinen, T. (1992) Pure absorption gradient enhanced heteronuclear single quantum correlation spectroscopy with improved sensitivity. *J. Am. Chem. Soc. 114*, 10663−10665.
(24) Delaglio, F., Grzesiek, S., Vuister, G. W., Zhu, G., Pfeifer, J., and Bax, A. (1995) NMRPipe: A multidimensional spectral processing system based on UNIX pipes. *J. Biomol. NMR 6*, 277−293.
(25) Johnson, B. A., and Blevins, R. A. (1994) NMRView: A computer program for the visualization and analysis of NMR data. *J. Biomol. NMR 4*, 595−740.
(26) Raffelberg, S., Mansurova, M., Gartner, W., and Losi, A. (2011) Modulation of the photocycle of a LOV domain photoreceptor by the hydrogen-bonding network. *J. Am. Chem. Soc. 133*, 5346−5356.
(27) Zoltowski, B. D., Vaccaro, B., and Crane, B. R. (2009) Mechanism-based tuning of a LOV domain photoreceptor. *Nat. Chem. Biol. 5*, 827−834.
(28) Christie, J. M., Corchnoy, S. B., Swartz, T. E., Hokenson, M., Han, I. S., Briggs, W. R., and Bogomolni, R. A. (2007) Steric interactions stabilize the signaling state of the LOV2 domain of phototropin 1. *Biochemistry 46*, 9310−9319.
(29) Song, S. H., Freddolino, P. L., Nash, A. I., Carroll, E. C., Schulten, K., Gardner, K. H., and Larsen, D. S. (2011) Modulating LOV domain photodynamics with a residue alteration outside the chromophore binding site. *Biochemistry 50*, 2411−2423.
(30) Lee, J., Tomchick, D. R., Brautigam, C. A., Machius, M., Kort, R., Hellingwerf, K. J., and Gardner, K. H. (2008) Changes at the KinA PAS-A dimerization interface influence histidine kinase function. *Biochemistry 47*, 4051−4064.
(31) Wu, Y. I., Frey, D., Lungu, O. I., Jaehrig, A., Schlichting, I., Kuhlman, B., and Hahn, K. M. (2009) A genetically encoded photoactivatable Rac controls the motility of living cells. *Nature 461*, 104−108.
(32) Baikalov, I., Schroder, I., Kaczor-Grzeskowiak, M., Grzeskowiak, K., Gunsalus, R. P., and Dickerson, R. E. (1996) Structure of the *Escherichia coli* response regulator NarL. *Biochemistry 35*, 11053−11061.
(33) Qin, Y., Luo, Z. Q., Smyth, A. J., Gao, P., Beck von Bodman, S., and Farrand, S. K. (2000) Quorum-sensing signal binding results in dimerization of TraR and its release from membranes into the cytoplasm. *EMBO J. 19*, 5212−5221.
(34) Pinto, U. M., and Winans, S. C. (2009) Dimerization of the quorum-sensing transcription factor TraR enhances resistance to cytoplasmic proteolysis. *Mol. Microbiol. 73*, 32−42.
(35) Zhu, J., and Winans, S. C. (2001) The quorum-sensing transcriptional regulator TraR requires its cognate signaling ligand for protein folding, protease resistance, and dimerization. *Proc. Natl. Acad. Sci. U.S.A. 98*, 1507−1512.